

Long-term Petrophysical Investigations on Geothermal Reservoir Rocks at Simulated In Situ Conditions

H. Milsch · A. Seibt · E. Spangenberg

Received: 3 August 2007 / Accepted: 27 June 2008 / Published online: 24 July 2008
© Springer Science+Business Media B.V. 2008

Abstract In the course of stimulation and fluid production, the chemical fluid–rock equilibrium of a geothermal reservoir may become disturbed by either temperature changes and/or an alteration of the fluid chemistry. Consequently, dissolution and precipitation reactions might be induced that result in permeability damage. In connection with the field investigations at a deep geothermal doublet, complementary laboratory-based research is performed to address these effects. The reservoir is located at a depth of 4100 to 4200 m near Groß Schönebeck within the Northeast German Basin, 50 km north of Berlin, Germany. Within the reservoir horizon, an effective pressure of approximately 45 MPa and a temperature of 150°C are encountered. Furthermore, the Lower Permian (Rotliegend) reservoir rock is saturated with a highly saline Ca–Na–Cl type formation fluid (TDS \approx 255 g/l). Under these conditions we performed two sets of long-term flow-through experiments. The pore fluid used during the first and the second experiment was a 0.1 molar NaCl-solution and a synthetic Ca–Na–Cl type fluid with the specifications as above, respectively. The maximum run duration was 186 days. In detail, we experimentally addressed: (1) the effect of long-term flow on rock permeability in connection with possible changes in fluid chemistry and saturation; (2) the occurrence and consequences of baryte precipitation; and (3) potential precipitations related to oxygen-rich well water invasion during water-frac stimulation. In all substudies petrophysical experiments related to the evolution of rock permeability and electrical conductivity were complemented with microstructural investigations and a chemical fluid analysis. We also report the technical challenges encountered when corrosive fluids are used in long-term in situ petrophysical experiments. After it was assured that experimental artifacts can be excluded, it is demonstrated that the sample permeability remained approximately constant within margins of $\pm 50\%$ for nearly six months. Furthermore, an effect of baryte precipitation on the rock permeability was not observed. Finally, the fluid exchange procedure did not alter the rock transport properties. The results of the chemical fluid analysis are in support of these

H. Milsch (✉) · E. Spangenberg
GeoForschungsZentrum Potsdam, Telegrafenberg, 14473 Potsdam, Germany
e-mail: milsch@gfz-potsdam.de

A. Seibt
Boden Wasser Gesundheit GbR., Seestr. 7a, 17033 Neubrandenburg, Germany

observations. In both experiments the electrical conductivity of the samples remained unchanged for a given fluid composition and constant p-T conditions. This emphasizes its valuable complementary character in determining changes in rock transport properties during long-term flow-through experiments when the risk of experimental artifacts is high.

Keywords Permeability · Rock transport properties · Hydrothermal fluid–rock interactions · Long-term petrophysical experiments · Geothermal reservoirs

1 Introduction

The purpose of this paper is to report the outcome of long-term flow-through experiments that complement the scientific efforts made by the GFZ-Potsdam on energy production from geothermal reservoirs ([http://www.gfz-potsdam.de/portal/-/?\\$part=CmsPart&\\$event=display&docId=1793765&cP=sec52.content.detail](http://www.gfz-potsdam.de/portal/-/?$part=CmsPart&$event=display&docId=1793765&cP=sec52.content.detail)). Within this framework a geothermal research doublet has been established at a site within the Northeast German Basin near Groß Schönebeck, 50 km north of Berlin, Germany.

The production and injection horizon is situated at 4100 to 4200 m depth and is composed of Lower Permian (Rotliegend) sandstones. The fault pattern analysis of a 3D structural model indicates normal to strike slip faulting for the Lower Permian sediments. The formation pore pressure (pp) is 43.8 MPa, determined by p-T logs at stationary conditions of the geothermal target horizon (Legarth et al. 2005). According to the stress relation of normal faulting the effective mean stress (σ_{meff}) was calculated as 42.9 MPa (Blöcher et al. 2008). The temperature at this location follows a normal geothermal gradient and is approximately 150°C. The pore fluid within the formation is of Ca-Na-Cl type with a high salinity (TDS \approx 255 g/l). Furthermore and in addition to other species, it has a non-negligible degree of mineralization with respect to Fe, Ba and SO₄ with concentrations typically around 67.6, 25.5, and 51.0 mg/l, respectively. A detailed description of the geological situation at this site can be found in Moeck et al. (2008).

In the course of reservoir stimulation and exploitation the local thermodynamic equilibrium of the formation is disturbed. This might induce a number of fluid–fluid and fluid–rock interactions potentially leading to permeability damage:

- (1) During reservoir stimulation by a water-frac, the formation fluid is displaced by oxygen-rich well water. This possibly causes the precipitation of iron hydroxides (Seibt 2000 and references cited therein). During the former procedure the temperature in the proximity of the injection well can be as low as 30°C.
- (2) After passing the binary power plant cycle, the cooled formation fluid might become oversaturated with respect to Ba²⁺ and SO₄²⁻. Thermodynamic calculations (CHEM-EQ) with the typical in situ concentration range indicated a positive saturation index (SI>0) for temperatures below 70°C (J. Bartels, personal communication, 2006). As this corresponds to the approximate fluid reinjection temperature, formation damage due to baryte precipitation is potentially promoted (Kühn et al. 1997; Dunn et al. 1999).
- (3) Finally, any alteration of fluid saturation with respect to the different ionic species of the rock minerals (e.g., Si) might induce dissolution-precipitation reactions within the formation in the course of fluid production (Aharonov et al. 1998; Tenthoery et al. 1998).

In contrast, an effect of clay swelling on the rock permeability (e.g., Omar 1990) in the present case is not to be expected, as the rock does not contain the relevant clay minerals. The preceding conditions and processes defined the experiments performed in this study.

Both theoretical and experimental studies with a related focus on the hydro-mechanical effect of mineral dissolution and precipitation reactions have previously been performed. They concerned primarily fluid assisted rock deformation also termed pressure solution (e.g., Rutter 1976; De Boer et al. 1977; Sprunt and Nur 1977; Gratier and Guiguet 1986; Tada et al. 1987). But investigations in the context of diagenesis (Small et al. 1992; Lemée and Guéguen 1996; Aharonov et al. 1998; Tenthorey et al. 1998), as well as fracture- (Yasuhara et al. 2006) and fault-gouge evolution (Giger et al. 2007), were also performed.

These investigations indicate that such reactions in fact can lead to a significant reduction in rock permeability by means of different grain scale mechanisms. The latter are governed by a complicated interrelationship of thermodynamic, mechanical, and fluid chemical parameters such as temperature, local stresses, and degree of ionic fluid saturation, respectively.

Dissolution and precipitation can occur both isolated and coupled. In connection with the present study it was previously shown (Tenthorey et al. 1998) that for low temperatures (<300°C) and homogeneous rock aggregates minerals other than quartz (e.g., feldspars) need additionally to be present. Here, the observed decrease in permeability was induced by authigenic clay phases that rapidly became precipitated after dissolution of the constituent ionic species and respective fluid oversaturation. In contrast, fracture aperture was also shown to decrease for a pure novaculite at low and moderate temperatures displaying in fact an underlying pure dissolution process (Yasuhara et al. 2006).

The aim of this research study was to experimentally investigate the occurrence and the effect of the particular processes (1) to (3) described above. This study was conducted under realistic conditions regarding rock and fluid types, combinations of confining and pore pressures, flow-rates and temperatures. The principal physical parameter investigated in the present study was the rock permeability. The latter was complemented by continuous measurements of the electrical sample conductivity as well as a chemical analysis of the pore fluid in regular time intervals. Finally, we describe the technical challenges encountered when using highly saline pore fluids over experimentally extremely long periods of time.

2 Experimental Methodology

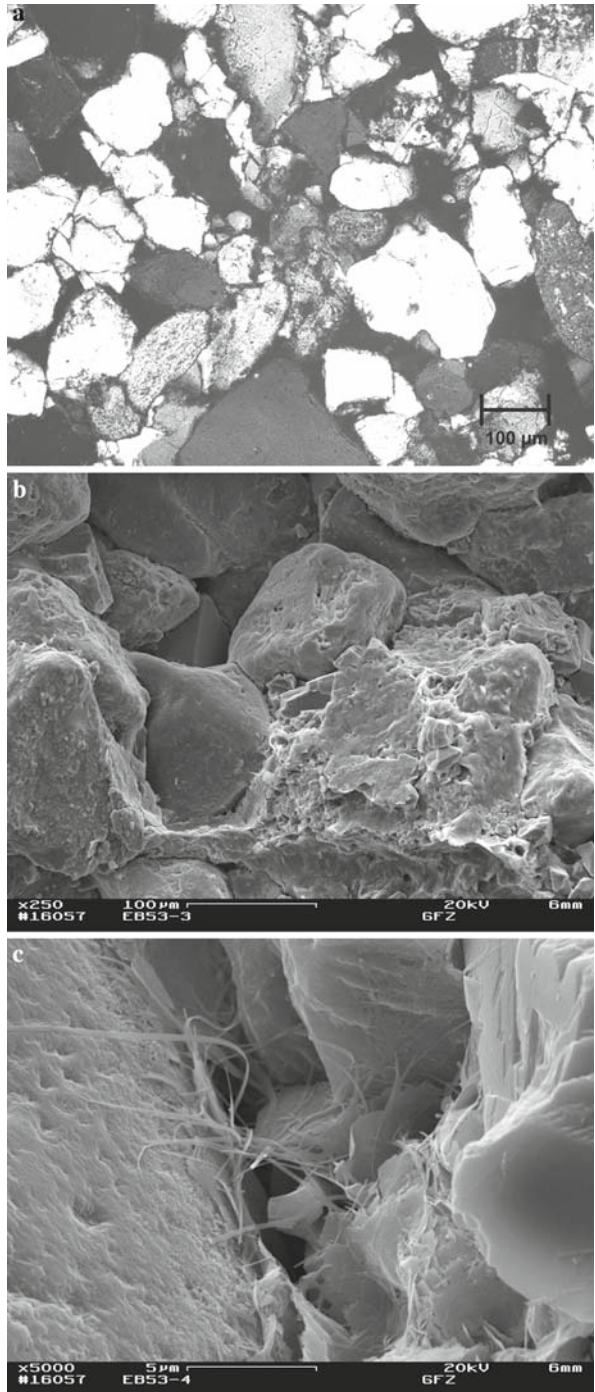
2.1 Sample Material and Fluids

The samples tested came from a prospective oil and gas well near Eberswalde/Germany (Eb 2/76). They were chosen for their mineralogical similarity with the aquifer rocks at the close by Groß Schönebeck site where no coring was performed. The specimens are Lower Permian (Rotliegend) sandstones of the Havel subgroup originating from a depth of approximately 4150 m.

Figure 1a shows an optical micrograph of the starting material (crossed nicols). The rock is an arcsoic litharenite and consists mainly of quartz (80 vol%). Quartz cement prevails (Fig. 1b). The quartz grains are often surrounded by iron (III) oxide-rims responsible for the reddish color of this type of sandstone. Carbonatic and albitic cements are rarely found. The average quartz grain size is 150 μm. The feldspar content is less than 10 vol%. K-feldspar sometimes partly albitised is predominant. Rock fragments are contained by less than 10 vol% and are mainly of volcanic origin. Sometimes an ophitic texture can be found. Accessory minerals are plagioclase, microcline and mica. Illite (Fig. 1c) and chlorite are the dominant clays.

For the experiments smaller cores were taken parallel to the bedding. Subsequently, surface grinding was performed to obtain samples with a cylindrical shape having a diameter

Fig. 1 (a) Optical micrograph (crossed nicols) of the starting material. The magnification is $100\times$. See text for more details on the sample microstructure. (b) SEM-image (BSE-mode) of broken sample (ebe05-3) showing quartz grains (center) and quartzitic cement (lower right). (c) SEM-image (BSE-mode) of broken sample (ebe05-3) showing fibrous illite growing into the pore space



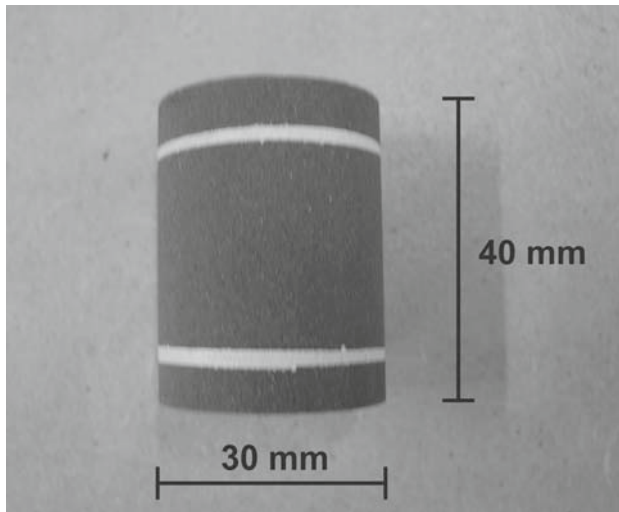


Fig. 2 Sample with silver paint rims at a distance of 25 mm for electrical conductivity measurements. The sample is 30 mm in diameter and 40 mm in length

of 30 mm and a length of 40 mm (Fig. 2). Two specimens labeled ebe05-3 and ebe05-4 were tested.

The fluids used were a 0.1 molar NaCl solution (sample ebe05-3) and a synthetic Ca–Na–Cl type formation fluid (sample ebe05-4). The latter aimed at simulating the in situ fluid of the Groß Schönebeck deep geothermal system (Giese et al. 2002) at this stage neglecting other ionic species. The fluid contains 99 g NaCl and 206 g $\text{CaCl}_2 \cdot 2\text{H}_2\text{O}$ (both reagent grade) per liter distilled water and thus a total amount of dissolved solids (TDS) of 255 g/l.

The fluid conductivities at 25°C are 10.8 mS/cm (NaCl solution) and 215 mS/cm (formation fluid), respectively, and were measured with a hand held conductivity meter (WTW Multi 340i with TetraCon 325 conductivity probe). A thorough description of the formation fluid viscosity dependence on temperature is given in Sect. 3.5.

2.2 Experimental Procedure

2.2.1 Generalities

The experiments were conducted under hydrostatic conditions in a recently set up HPT-permeameter. The apparatus and details of measurement procedures are described in our companion paper (Milsch et al. 2008). Electrical conductivity measurements were performed in a four-electrode arrangement with a variable shunt-resistor. For this purpose silver rims were painted onto the dried samples at a distance of 25 mm prior to immersion with their respective fluids under vacuum (Fig. 2). The latter procedure also served for determining the starting porosity by comparing the dry and wet sample masses.

To reduce the risk of corrosion within the apparatus the synthetic formation fluid was flushed with nitrogen for 12 h to minimize its oxygen content, was then filled into the evacuated pore pressure system, and was finally prepressurized with nitrogen to 0.2 MPa. After assembly, the specimens were subjected to a confining and a pore pressure of 10 and 5 MPa and a temperature of 30°C, respectively, defining the starting conditions.

Given a full stroke volume of 265 ml the active upstream pore fluid pump was refilled approximately once per day with the respective fluid. The flow was unidirectional and repeated pumping of the same fluid was not performed. Despite the ability of the apparatus to perform a continuous fluid flow with four pumps, only one upstream and one downstream pump were active at the same time. The other two were kept on hold and they took over when servicing of the former ones had become necessary. Particularly, this was the case when at a given point leakage occurred due to pump seal damage as a consequence of salt crystallization on the pump cylinder walls.

2.2.2 Long-term Experiment with 0.1 Molar NaCl Solution

The long-term flow-through experiment with sample ebe05-3 was conducted over 45 days. A continuous flow-rate of 0.1 ml/min was applied. After confining pressure increase to 50 MPa the temperature was maintained at 30°C for 2 days and was then increased to 150°C for the remainder of the experiment. The confining and pore pressures were kept constant at 50 and 5 MPa, respectively.

For this sample, SEM microstructural analysis including EDX (Energy Dispersive X-ray) element mapping for Si, Al, Fe, K, Ca, and S has been performed after the experiment (Zeiss DSM 962 with Noran/Tracor Voyager 2.6).

2.2.3 Long-term Experiment with Synthetic Formation Fluid

The long-term flow-through experiment with sample ebe05-4 had a total duration of 186 days. The flow-rate was 0.1 ml/min and the test was performed at constant confining and pore pressures of 50 and 5 MPa, respectively. After confining pressure increase to 50 MPa the temperature was maintained at 30°C for three days and was then increased to 150°C. After 30 and 83 days the flow was stopped and the sample was maintained at stable p-T conditions for 45 and 81 days, respectively. After these hold periods, flow was resumed for approximately 7 days each.

2.2.4 Fluid Exchanges

Subsequent to this first experimental stage with sample ebe05-4, the fluid was enriched with progressively increased concentrations of Ba^{2+} and SO_4^{2-} ions by adding specific amounts of 0.1 molar BaCl_2 and Na_2SO_4 solutions to the synthetic formation fluid.

Three different concentrations $n(\text{Ba}^{2+}):n(\text{SO}_4^{2-})$ [n in mM/l] were tested: (1) 0.19:0.19; (2) 0.19:0.57, and (3) 0.38:1.14. This covers the in situ Ba^{2+} concentrations and $n(\text{Ba}^{2+}):n(\text{SO}_4^{2-})$ ratios of the Groß Schönebeck formation fluid which are in the range of 0.19 to 0.44 mM/l and 1:1 to 1:3, respectively. This flow-through test had a duration of 7 days and was performed at a temperature of 60°C.

The fluid was then exchanged at 150°C against tap water acidified to pH 5 with acetic acid and the temperature was then, again, decreased to 60°C and then further to 30°C. The flow with tap water was maintained for 5 days. At the end of this experimental stage the tap water was finally exchanged against the original synthetic formation fluid, and the temperature was increased to 150°C to establish the starting conditions for comparison.

Table 1 Sample properties at starting conditions

Sample Nr.	Porosity (%)	Permeability (m ²) pc = 10 MPa	Permeability (m ²) pc = 50 MPa	Conductivity (mS/cm) pc = 10 MPa	Conductivity (mS/cm) pc = 50 MPa
ebe05-3	12.3	$0.45 \cdot 10^{-15}$	$0.33 \cdot 10^{-15}$	0.32	0.26
ebe05-4	11.1	$4.9 \cdot 10^{-15}$	$2.0 \cdot 10^{-15}$	5.0	3.8

The pore pressure was 5 MPa and pc denotes the confining pressure. The specific electrical conductivity is given at a temperature of 30°C

2.2.5 Chemical Fluid Analysis (Sample ebe05-4)

For sample ebe05-4 the total amount of fluid that had transversed the sample during 60 days of flow was 8.6 l. During both stages of this experiment a total of 30 fluid samples were taken, generally one every second day during times of flow. The samples contained approximately 150 ml of fluid each. Immediately after release the fluid pH and redox potential Eh were measured at ambient p-T conditions (WTW Multi 340i with Mettler-Toledo probes InLab 412 (pH) and InLab 501 (Eh)).

The fluid samples were then chemically analyzed for cation and anion concentrations of Fe, Mn, Al, Zn, Cu, Pb, K, Si, Ba, and SO₄, respectively. Besides Fe and Mn, which were analyzed photometrically, chemical analysis was performed by either GF-AAS (Graphite Furnace Atomic Absorption Spectrometry; Al, Zn, Cu, Pb) or by ICP-MS (Inductively Coupled Plasma Mass Spectrometry; K, Si, Ba, and SO₄ through S) at VKTA Rossendorf e.V. Here, the detectable minimum concentrations, taking dilution into account, were 50 μg/l (Al, Zn), 10 μg/l (Cu, Pb, K), 60 μg/l (Si), 5 μg/l (Ba), and 1500 μg/l (SO₄), respectively. For this sample no post-experimental analysis of the microstructure was possible due to an O-ring failure upon depressurization.

2.2.6 Procedural Overview

Table 1 summarizes the sample properties at starting conditions and after the confining pressure increase to 50 MPa, the porosity being measured at ambient pressure as described above. This table emphasizes the significant effect of an effective pressure increase on both transport properties. Effective pressure is meant as the difference between the confining and pore pressures according to Terzaghi's Principle (Terzaghi 1923).

The flow chart in Table 2 summarizes the procedures of the experiments for both samples tested.

3 Experimental Results

3.1 Long-term Experiment with 0.1 Molar NaCl Solution

The measured permeability and electrical conductivity are shown in Figs. 3 and 4, respectively, as a function of time. The increase in electrical conductivity after 2 days is due to the temperature increase from 30 to 150°C. After 4 days the permeability started to decrease from $0.33 \cdot 10^{-15} \text{ m}^2$ to a minimum of $1.0 \cdot 10^{-17} \text{ m}^2$. This decrease was interrupted by short permeability jumps back toward its initial value. As the electrical conductivity remained

Table 2 Flow chart of the experimental procedure

Sample ebe05-3 0.1 molar NaCl-fluid	Sample ebe05-4 Synthetic formation fluid (TDS = 255 g/l)
Stage 1: Long-term flow-through experiment T = 150°C, pc = 50 MPa, pp = 5 MPa Measured parameters: $k, \sigma = f(t)$ Duration: 45 days, $Q = 0.1$ ml/min	Stage 1: Long-term flow-through experiment T = 150°C, pc = 50 MPa, pp = 5 MPa Measured parameters: $k, \sigma = f(t)$ Duration: 170 days, $Q = 0.1$ ml/min Stage 2: Fluid exchanges pc = 50 MPa, pp = 5 MPa Measured parameters: $k, \sigma = f(t)$ (A) synthetic formation fluid + three different concentrations of Ba and SO ₄ ions T = 60°C (B) tap water acidified to pH 5 T = 60 and 30°C Duration: 16 days, $Q = 0.1$ ml/min

k , permeability; σ , electrical conductivity; t , time; pc, confining pressure; pp, pore pressure; T, temperature; Q , flow-rate

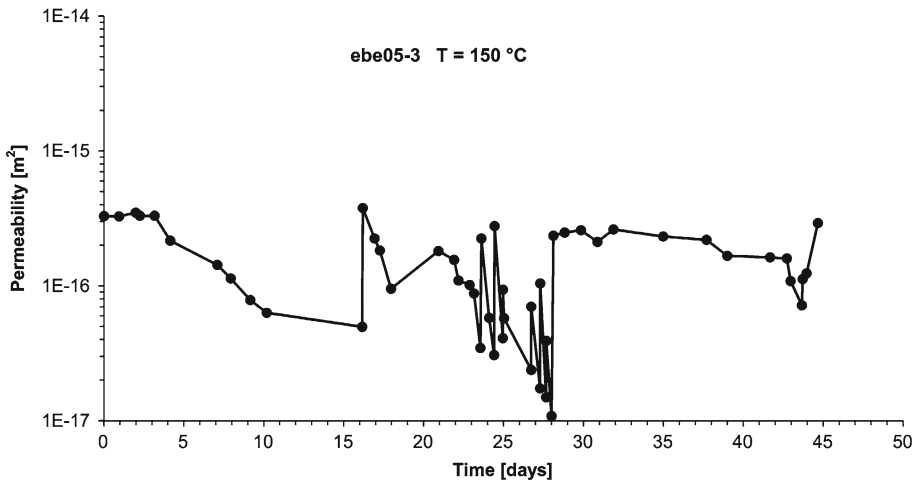


Fig. 3 Sample ebe05-3. Permeability as a function of time. Permeability fluctuations are due to rust deposit on the upstream side of the sample. After flushing with distilled water at 28 days, the permeability remained more or less constant at approximately 20% below its initial value

unchanged it was supposed that some kind of clogging had occurred at the upstream side of the sample as both parameters are related at least qualitatively (Table 1 and e.g., [Martys and Garboczi 1992](#)).

The sample was then flushed with distilled water after 28 days leading to both the marked decrease in electrical conductivity and the dramatic increase in permeability to approximately 20% below its original value. Flow with the original fluid was then resumed. For the remainder of the experiment the permeability continued to decrease by 40% but this time slower and more or less steadily. In contrast, the electrical conductivity showed a minor increase by approximately 5%. At the end of the experiment between 43 and 45 days the changes in

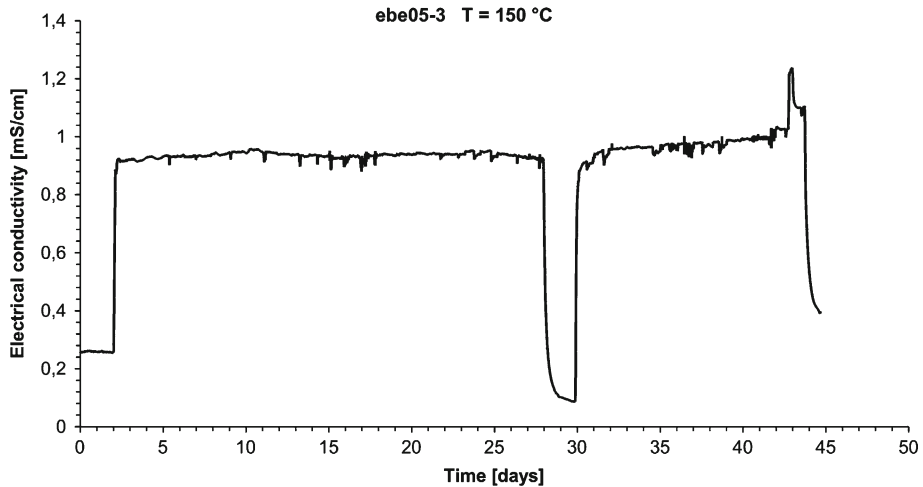


Fig. 4 Sample ebe05-3. Electrical conductivity as a function of time. Significant changes in electrical conductivity at stable p-T conditions (2–43 days) were not observed. This supports the conclusion of unaltered transport properties of the sample in the course of the experiment. The decrease in electrical conductivity at 28 days is due to sample flushing with distilled water

both transport properties are induced by a decrease in confining pressure from 50 to 10 MPa and a decrease in temperature from 150 to 40 °C, respectively, after which the measurement has been stopped. The trend in electrical conductivity is plausible and physically connected to the changes in both parameters whereas the permeability appears unrelated. In fact, the upstream side of the dismantled sample showed a brownish mud like cover that very likely consisted of iron hydroxide.

3.2 Long-term Experiment with Synthetic Formation Fluid

The iron hydroxide originated from one single corrosive spot within the pore pressure system at the thread of one of the reservoir tanks. To avoid further corrosion, the synthetic formation fluid and the pore pressure system were preconditioned as described in Sect. 2.2.1.

The evolution of both permeability and electrical conductivity during the first stage of this experiment is shown in Figs. 5, 6a,b, respectively, as a function of time. The decrease of both transport properties after start from $4.9 \cdot 10^{-15}$ to $2.0 \cdot 10^{-15}$ m² and from 5.0 to 3.8 mS/cm, respectively, is due to a confining pressure increase from 10 to 50 MPa. The conductivity increase from 3.8 to approximately 11.0 mS/cm after 4 days from start is due to a temperature increase from 30 to 150 °C.

For the next 26 days the sample was continuously flown through. Within experimental errors (e.g., a time dependent minor leak of the upstream pump) the permeability remained constant at $2.2 \pm 0.8 \cdot 10^{-15}$ m². The two longer hold phases were introduced for comparison by allowing a chemical equilibration of the fluid with the rock. Additionally, they gave the opportunity to service the pore fluid pumps in regular time intervals. Flow was resumed after 76 days from start. Compared to the situation before, the permeability had decreased by approximately 50% to $0.9 \pm 0.1 \cdot 10^{-15}$ m². In contrast, it remained nearly constant for the remainder of the experiment.

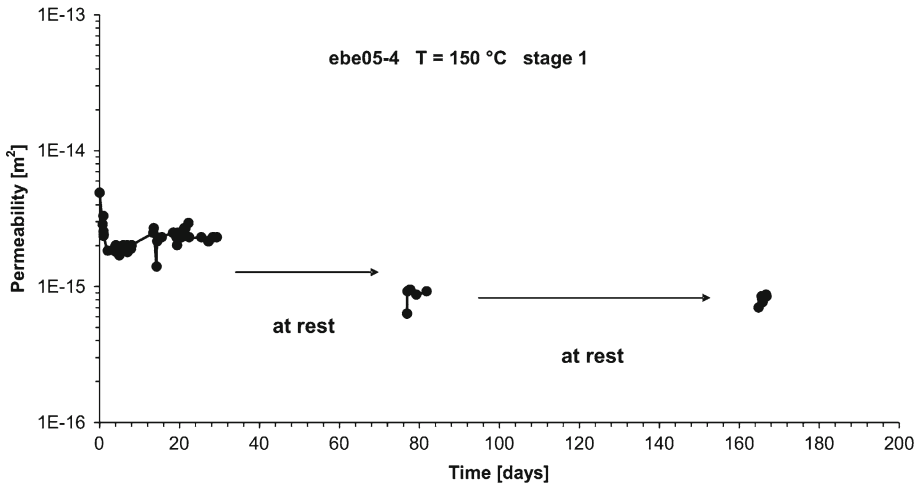


Fig. 5 Sample ebe05-4, stage 1. Permeability as a function of time. During the three periods of flow at stable p-T conditions (4–170 days) the permeability remained constant within margins of approximately $3 \cdot 10^{-15} \text{ m}^2$ and $1 \cdot 10^{-15} \text{ m}^2$, respectively. For an interpretation of the permeability offset after the first hold see Sect. 4.3 for more details

By the use of a highly saline fluid the electrical conductivity showed a substantial scatter (Fig. 6a). Interestingly, this noise was reversibly not observed when the temperature was below approximately 100°C . Furthermore, it showed that the signal sharply alternated between an upper and a lower level of $10 \pm 1.0 \text{ mS/cm}$ during the second and third flow phases. An abrupt switching of the conductivity value also becomes evident when the signal is time averaged in 24-h intervals (Fig. 6b) compared to a normal sampling rate of 2 per minute. This figure finally demonstrates that the electrical conductivity remains unaltered in the course of the experiment at stable p-T conditions within margins of approximately $\pm 10\%$.

3.3 Fluid Exchanges

The Figs. 7, 8, and 9 show the temperature, permeability, and electrical conductivity, respectively, as a function of time in the course of the second stage of the experiment with sample ebe05-4.

The lowest concentration of Ba^{2+} and SO_4^{2-} ions was added to the pure formation fluid at a temperature of 150°C and the latter was then decreased to 60°C . For each of the three different concentrations the flow was maintained for 2–3 days. Subsequently, this fluid was exchanged against tap water at 150°C which then was flown through the sample at 60, 30, and 60°C , respectively, for approximately 1 day at each temperature level. Finally, the tap water was exchanged against the original, pure formation fluid to establish the starting conditions both at 150°C and then at 30°C .

As a result, neither a change in temperature nor the different fluid exchanges affected the sample permeability, which remained constant at approximately $1 \pm 0.1 \cdot 10^{-15} \text{ m}^2$. The evolution of the sample permeability during both experimental stages with specimen ebe05-4 is summarized in Fig. 10.

In Fig. 9 the conductivity curve closely follows the temperature plot in Fig. 7 unless the fluid is tap water. Here, naturally, the electrical conductivity of the sample is close to zero (0.06 mS/cm). By comparison, it is evident that the electrical conductivity—for a given

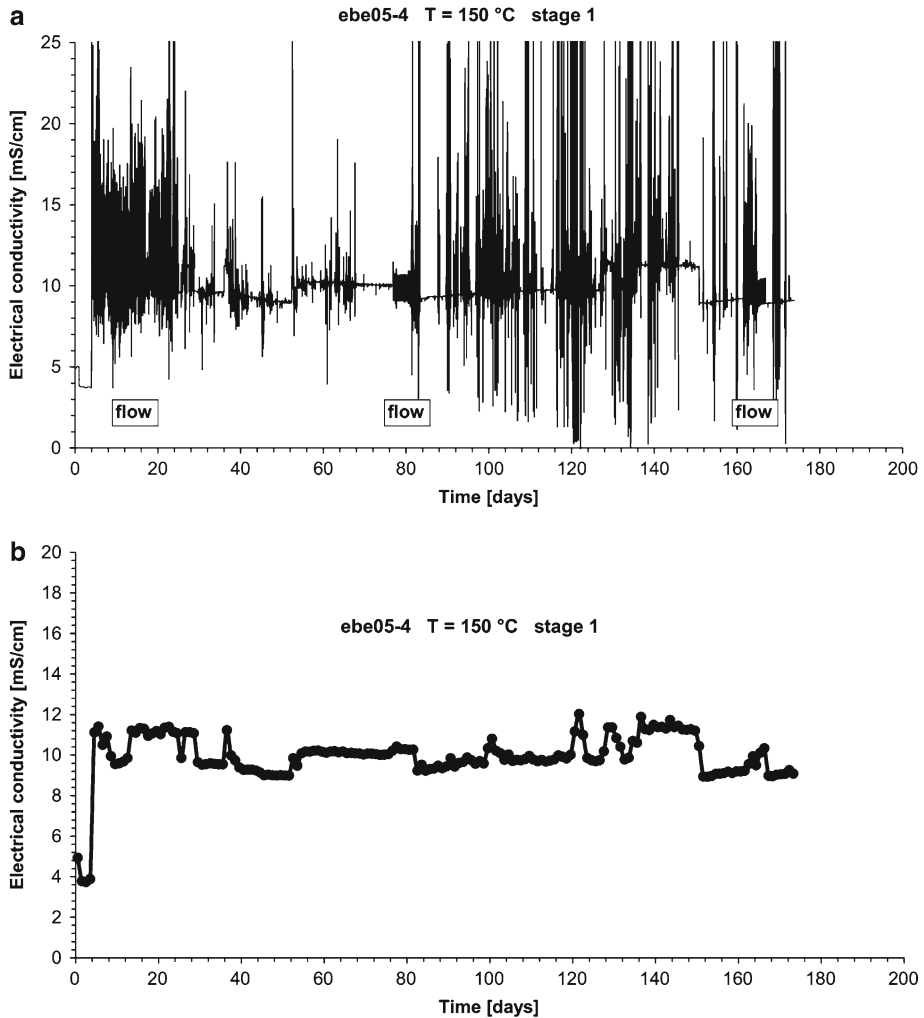


Fig. 6 (a) Sample ebe05-4, stage 1. Electrical conductivity as a function of time. Due to the high salt content of the synthetic formation fluid, the electrical conductivity signal became reversibly disturbed above temperatures of approximately 100°C. During flow after the first and second hold the signal alternated sharply between a lower and an upper level of 9 and 11 mS/cm, respectively. (b) Sample ebe05-4, stage 1. As in (a) but the signal was time-averaged over 24 h. Here, signal alternation becomes more apparent. In addition, the graph evidently indicates the constancy of the electrical sample conductivity within margins of 10 ± 1.0 mS/cm. In connection with the permeability measurement this supports the conclusion of unaltered sample transport properties in the course of the experiment within experimental limits

temperature and fluid composition—was not altered at either stage of this fluid exchange procedure. In addition, the conductivity value at 30°C and 16 days in Fig. 9 (3.6 mS/cm) matches the one measured more than 180 days before within 5%.

Both measurements with the formation fluid at 150°C highlight the obvious sharply defined conductivity band when this type of fluid is in motion at higher temperature. It can also be seen that this scattering signal reversibly vanishes and reoccurs depending on the temperature level.

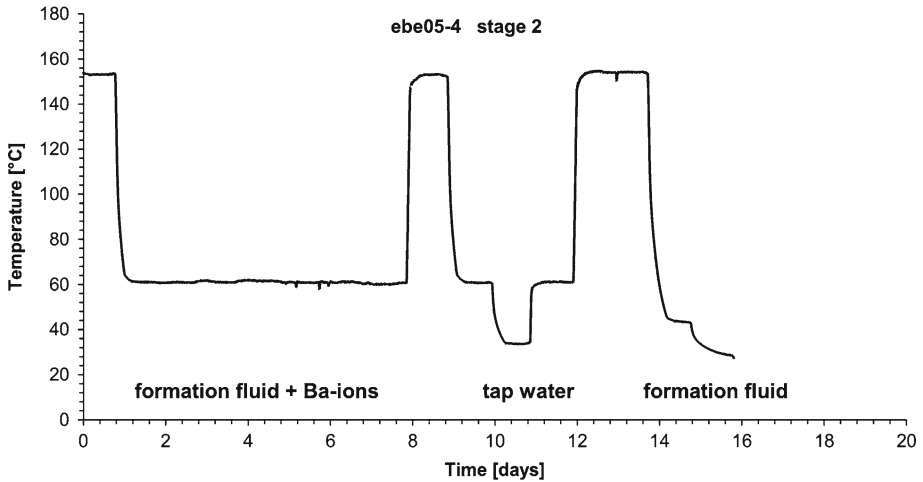


Fig. 7 Sample ebe05-4, stage 2. Temperature as a function of time during the fluid exchange procedure. During fluid exchange the formation fluid was first enriched with Ba^{2+} and SO_4^{2-} ions and was then replaced by tap water acidified to pH 5

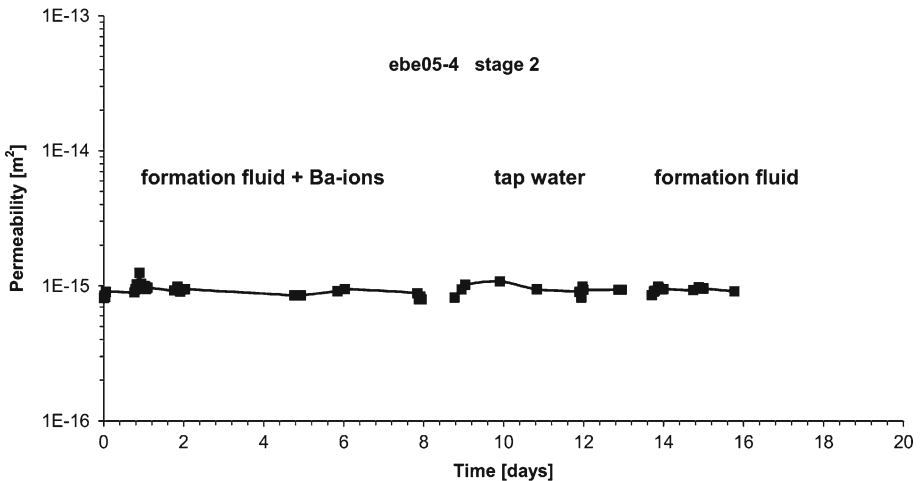


Fig. 8 Sample ebe05-4, stage 2. Permeability as a function of time. Neither a change in temperature nor the different fluid exchanges affected the sample permeability which remained constant at approximately $1 \pm 0.1 \cdot 10^{-15} \text{ m}^2$

Finally, it is worth to note that the full fluid exchange of the formation fluid against tap water and vice versa took approximately 24 h as evidenced by the conductivity signal. In contrast, for a flow-rate of 0.1 ml/min, a sample volume of 28 cm^3 , and a porosity of approximately 11% the former could have been accomplished within 30 min.

3.4 Chemical Fluid Analysis (Sample ebe05-4)

The formation fluid pH before the onset of the experiment was 5.5 at 21.9°C . The post-experiment formation fluid samples had pH values in the range of 5.1–6.6 at 20.0°C with

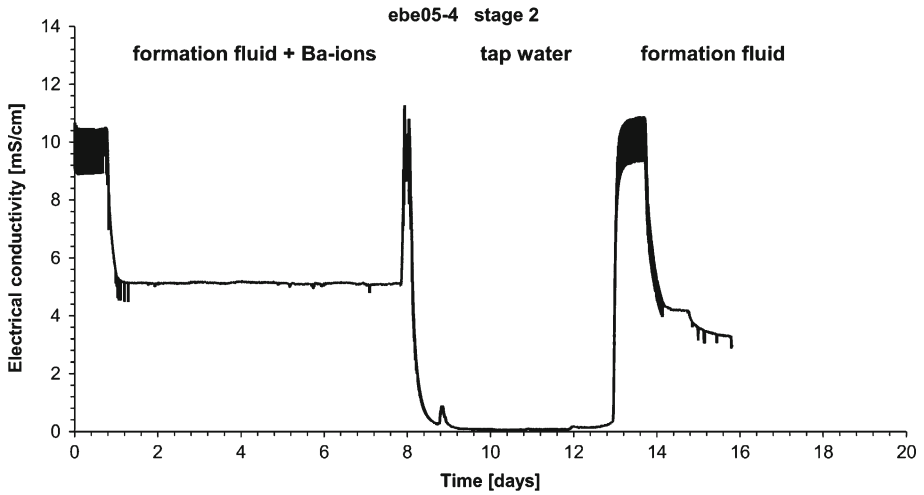


Fig. 9 Sample ebe05-4, stage 2. Electrical conductivity as a function of time. At stable p-T and fluid compositional conditions the electrical sample conductivity remained constant. Note the sharply alternating signal when flow was performed with the formation fluid at 150°C. Also note that the exchange of formation fluid against tap water and vice versa took approximately 24 hours. This is significantly longer than expected for the given flow-rate (0.1 ml/min) and the sample porosity (11.1%)

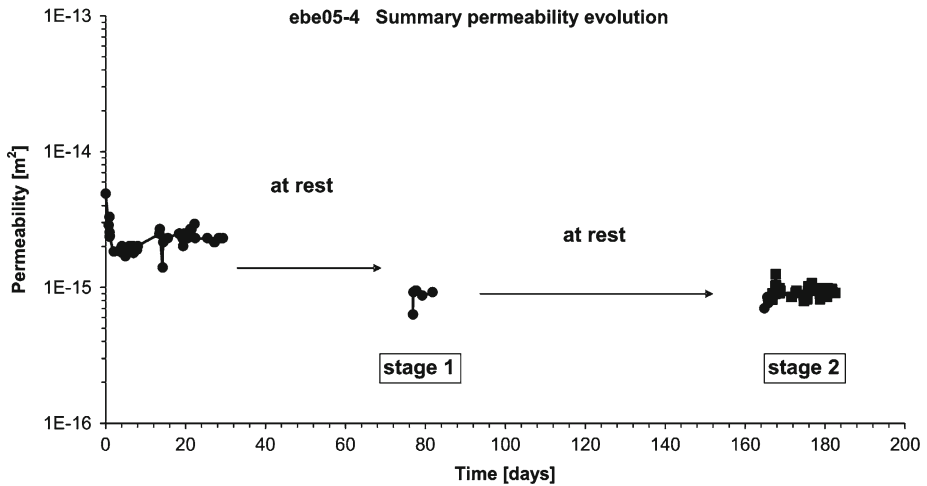


Fig. 10 Sample ebe05-4, both stages. Summary of the permeability evolution of the sample as a function of time for comparison

no systematic trend. The redox potential measurements yielded inconsistent results and will therefore not be discussed.

Fe and Mn, both measured photometrically, yielded concentrations of 1.72 ± 0.87 and 1.76 ± 0.78 mg/l, respectively. The former was the highest right at the beginning of the test after the temperature had been increased to 150°C and slightly decreased in the course of the experiment. For the Mn concentration no systematic trend was observed. The principal

Table 3 Results of the chemical fluid analysis (sample ebe05-4)

Fluid sample number	Days from start	Si (mg/l)	K (mg/l)	Ba (mg/l)	SO ₄ (mg/l)	Al (mg/l)	Cu (mg/l)	Zn (mg/l)	Pb (mg/l)	Fluid
Reference	0	0.39	6.5	0.1	11.0	<0.05	0.102	<0.05	0.020	ff
3	5	32.3	28.4	39.1	61.5	<0.05	1.000	0.216	1.040	ff
5	7	23.6		30.5	51.6					ff
8	14	29.4		60.3	88.8					ff
10	19	26.4		51.9	77.7					ff
16 after hold	78	31.4	9.9	33.2	52.5	<0.05	0.418	<0.05	0.049	ff
17a after hold	166	32.0	0.9	31.4	48.6	<0.05	0.189	<0.05	0.032	ff
18	174	17.2		21.8	33.9					(1)
19	175	12.2		29.9	37.8					(1)
20	178	6.2		28.6	54.3					(2)
21	179	2.1		31.4	128.0					(3)
22	180	2.6		25.9	69.6					ff
23	181	1.6		17.3	42.6					ff

ff: Pure formation fluid

(1) $\text{ff} + n(\text{Ba}^{2+}) = 0.19 \text{ mM/l} + n(\text{SO}_4^{2-}) = 0.19 \text{ mM/l}$

(2) $\text{ff} + n(\text{Ba}^{2+}) = 0.19 \text{ mM/l} + n(\text{SO}_4^{2-}) = 0.57 \text{ mM/l}$

(3) $\text{ff} + n(\text{Ba}^{2+}) = 0.38 \text{ mM/l} + n(\text{SO}_4^{2-}) = 1.14 \text{ mM/l}$

results of the chemical fluid analysis performed with GF-AAS and ICP-MS are listed in Table 3 and will be discussed in Sect. 4.5.

3.5 Determination of the Formation Fluid Viscosity by Permeability Measurements

As described in Milsch et al. (2008) the permeability k of a rock in the present case is determined by a steady state method making direct use of Darcy's Law (e.g., Darcy 1856; Scheidegger 1974; Bear 1988):

$$k = \frac{q\eta\Delta l}{\Delta p}, \quad (1)$$

where q , η , Δl and Δp denote, in this order, the fluid volume flux (the Darcy velocity), the (dynamic) fluid viscosity, the sample length and the pressure difference.

Thus, the permeability determination relies on the pressure difference measured over the sample. For a given flow-rate, cross-sectional area, sample length, and permeability, the pressure difference measured will depend on the fluid viscosity. Since the pressure difference was observed to remain unaltered for a given fluid composition and temperature, the unknown temperature dependence of the formation fluid viscosity can be calculated.

The latter is accomplished by comparing the pressure differences of both tap water and formation fluid measured during temperature ramping (Fig. 7). Under the assumptions made above, the formation fluid viscosity (at 5 MPa) is then given by:

$$\eta(\text{ff}, T) = \frac{\Delta p(\text{ff}, T)}{\Delta p(\text{tw}, T)} \eta(\text{tw}, T), \quad (2)$$

where $\eta(\text{ff}, T)$, $\eta(\text{tw}, T)$, $\Delta p(\text{ff}, T)$, and $\Delta p(\text{tw}, T)$ denote, in this order, the unknown formation fluid viscosity, the viscosity of tap water assumed to be equal to that of pure water, the

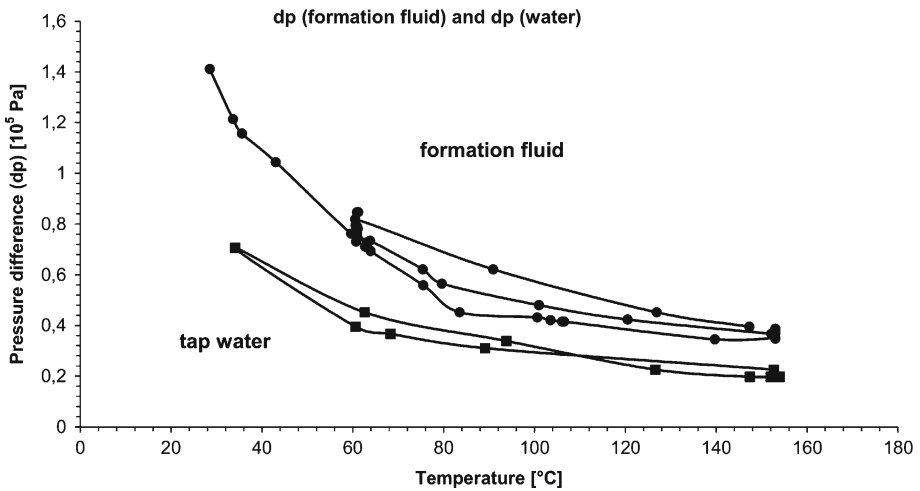


Fig. 11 Sample ebe05-4. Pressure differences measured for both formation fluid and tap water during the fluid exchange procedure in stage 2 as a function of temperature. This data was used to calculate the unknown temperature dependence of the formation fluid viscosity (Fig. 12) according to Eq. 2 in Sect. 3.5

pressure difference measured with the formation fluid, and the pressure difference measured with tap water. All values refer to an individual temperature T .

In Fig. 11 both pressure differences are shown as a function of temperature. For the formation fluid the scatter of the measured values above 60°C is due to a minor leak of the upstream pump. For the viscosity calculation according to Eq. 2 averaged pressure difference values were used. The temperature dependence of the viscosity of pure water at 5 MPa fluid pressure was calculated with the NIST program REFPROP.

Figure 12 shows both viscosity-temperature dependences so derived. All permeability values presented in this paper were calculated according to the fluid-temperature conditions referring to one of the two graphs. The formation fluid viscosity was also directly measured at 20°C and ambient pressure with a Höppler-viscosimeter. The value obtained was 1.72 ± 0.05 mPa s, which is in excellent agreement with the one estimated by extrapolating the respective graph in Fig. 12 to 20°C .

4 Discussion

4.1 Experimental Aspects

Technically, it has been shown that flow-through experiments of significant length (6 months) at elevated p - T conditions are feasible. However, two principal difficulties in connection with the use of brines have been encountered. Despite a thorough material selection throughout the apparatus, corrosion could not be totally avoided. As a result, an artificial permeability decrease was observed during the first of two tests that was related to rust deposit on the upstream side of the sample. In the subsequent experiment this problem was successfully circumvented by minimizing the oxygen content within the pore pressure system through N_2 -flushing of the pore fluid.

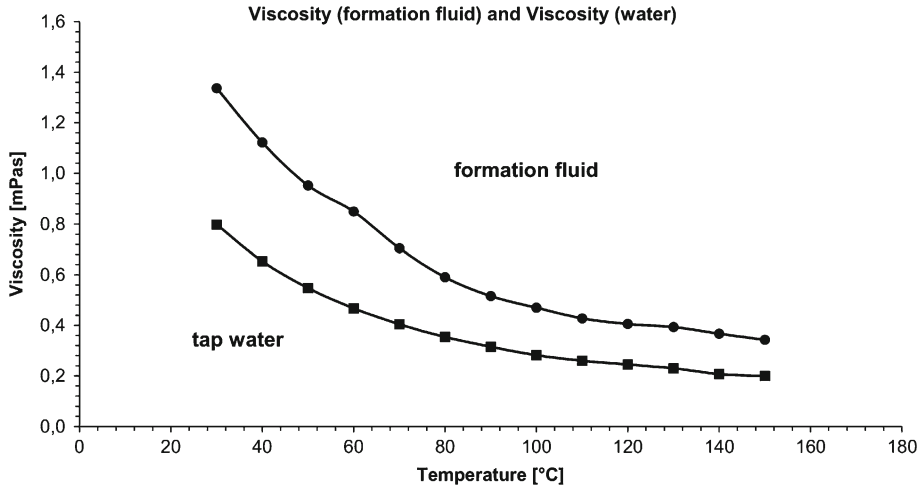


Fig. 12 Sample ebe05-4. Viscosity of both formation fluid and tap water as a function of temperature. See Sect. 3.5 for more details. All permeability values presented in this paper were calculated according to the fluid-temperature conditions referring to one of the two graphs

In contrast, high salt contents of the fluid are a persistent challenge for the (dynamic) pore fluid pump seals. The deposit of salt on the pump cylinder walls favors leakage. Regular servicing of the pumps thus becomes necessary. The use of two active pumps and two pumps on hold were proven to allow an uninterrupted fluid flow.

In this context it was shown that, despite generally different microstructural scale dependences, complementary electrical conductivity measurements are valuable for separating true from artifactic permeability changes. In addition, the electrical conductivity and thus potentially evolving rock transport properties are also monitored when the fluid is stationary.

4.2 Determination of the Formation Fluid Viscosity by Permeability Measurements

We presented a method for deriving an unknown fluid viscosity and its temperature dependence through permeability measurements. The measurement relies on the applicability of Darcy's Law and requires a second fluid with known properties for comparison. Despite the exploratory character of the method within the present study, the viscosity so determined was in excellent agreement with an independent measurement performed at 20°C. The technique has the advantage that no secondary experimental setup is required, as the measurement is performed directly with the sample to be investigated regarding its permeability. The method can yield accurate results when it is ensured that no leakage occurs and that the permeability in fact remains unaltered during fluid exchange. Precision in the present case is favored by the excellent flow stability, pressure resolution, and temperature stability provided by the apparatus.

4.3 Evolution of the Sample Transport Properties

Based on the measurements performed it is concluded that during neither long-term experiment with an isochemical fluid composition any real and significant alteration of the transport properties had occurred.

For the test with sample ebe05-3 this is supported by the fact that the permeability increases dramatically toward its initial value once the fluid breaks through the rust cover at the upstream side of the sample when the pressure gradient becomes high enough.

For the experiment with sample ebe05-4 this conclusion is directly supported by the permeability measurements themselves. During the three periods of flow at stage 1 the permeability remains constant within an upper and a lower limit of approximately $3 \cdot 10^{-15} \text{ m}^2$ and $1 \cdot 10^{-15} \text{ m}^2$, respectively. The permeability offset after the first hold is then interpreted to be due to residual rust within the pore fluid system that has been deposited on the upstream side of the sample after flow was resumed. In connection with the constancy of the sample permeability for the remainder of this stage of the experiment, we suggest that other processes like fines migration, clay break-up and/or mineral precipitation are negligible with respect to their effect on rock permeability.

Also during stage 2 no further change in sample permeability was observed. For baryte precipitation this is evidently due to an insufficient Ba^{2+} and SO_4^{2-} concentration. In addition, precipitation experiments (A. Seibt; unpublished data) indicate that baryte nucleation is significantly retarded when the fluid is in motion. For the fluid exchange against tap water this indicates that an effect on the rock transport properties is only to be expected when the replaced formation fluid contains a significant amount of ionic species to be oxidized (e.g., Fe^{2+}).

4.4 Microstructural Evolution and EDX Analysis (Sample ebe05-3)

The post-experimental microstructure of sample ebe05-3 showed no obvious departure from the one investigated before start. Particularly, no significant infiltration of corrosion-related rust into the specimen had occurred as evidenced by both optical- and SE-microscopy.

Figure 13 shows an EDX element map taken for Si, Al, and Fe on a broken part of the sample oriented perpendicular to the flow direction and taken at a distance of approximately 5 mm from the upstream side of the specimen. Fe is only present as traces mainly related to smaller amounts of iron (III) oxide preserved on the quartz grains. Si dominates due to the high quartz content of the sample. Al is related to both K-feldspar and clay minerals (mainly illite and chlorite). A minor K-peak observed in the EDX-spectrum emanated from the former mineral. Ca and S were not detected indicating the absence of carbonatic cement and anhydrite within the resolution limits.

Although the observed permeability decrease here was artifactic these results indicate that an entire sample can become impermeable in the direction of flow when relevant amounts of precipitates induce pore clogging even with no significant spatial extent in terms of infiltration depth.

4.5 Chemical Fluid Analysis (Sample ebe05-4)

The results of the chemical analysis indicate that ionic species of K, Cu, Zn and Pb that have been residually preserved within the sample after initial coring become easily dissolved and flushed-out after flow has been started. No dissolution of Al was observed despite the presence of K-feldspar as well as illite and chlorite as the principal clay minerals within the samples.

Si maintained an approximately constant (equilibrium) concentration of 30 ppm (stage 1) regardless of the flow situation. The former appears to be affected by the presence of Ba^{2+} and/or SO_4^{2-} ions when the latter were introduced artificially (stage 2). In their experiments [Tenthorey et al. \(1998\)](#) observed a four times higher Si equilibrium concentration in pure

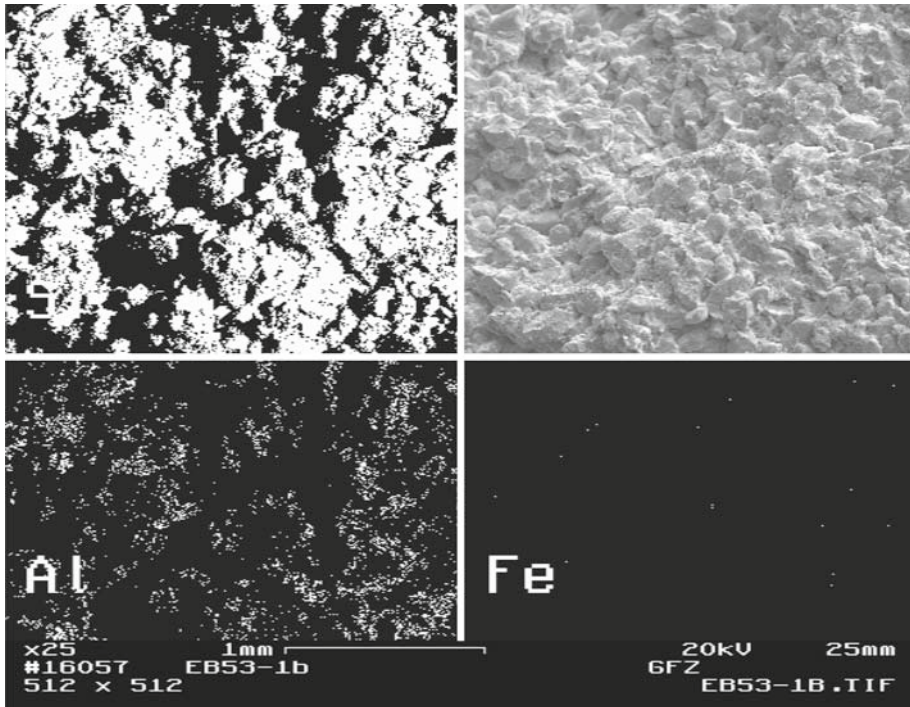


Fig. 13 Results of post-experimental EDX element mapping for Si, Al and Fe (sample ebe05-3). Si prevails due to the high quartz content of the sample. Al emanates from both K-feldspar and clay minerals (mainly illite and chlorite). The Fe content is very low and mainly related to smaller amounts of iron (III) oxide preserved on the quartz grains. See text for more details

water at a comparable temperature. Besides significant differences in fluid composition this might be due to the fact that their fluid volume was limited (6 ml) and was cycled back and forth through the sample potentially becoming more enriched in Si in terms of a true equilibrium concentration.

An approximately constant $n(\text{Ba}^{2+}):n(\text{SO}_4^{2-})$ ratio of $1:2.2 \pm 10\%$ was observed during stage 1 and thus prior to the enrichment of the formation fluid with these species. This indicates the preservation of baryte precipitates after initial core recovery or the presence of smaller amounts of baryte cement. Consequently, no effect of precipitation was observed during stage 2 for a molar ratio of 1:1. Despite a progressive relative depletion in Ba^{2+} ions (fluid sample 21), the SO_4^{2-} concentration measured indicates that barite precipitation can also be excluded for the lowest $n(\text{Ba}^{2+}):n(\text{SO}_4^{2-})$ ratios investigated in the present study.

In summary, these results suggest that dissolution of various species including quartz is viable and could even result in an increase in sample permeability. In contrast, an effect of potential precipitation reactions on the rock transport properties appears negligible under the conditions investigated.

5 Conclusions

We conducted long-term flow-through experiments to investigate risks of permeability damage related to fluid–rock interactions and specifically to dissolution and precipitation

reactions. Besides experiments performed with a nominally isochemical fluid composition, potential effects of both baryte precipitation and well water injection during reservoir stimulation were investigated. The effective pressure and temperature conditions applied and the rock and fluid types chosen aimed at simulating the setting within a geothermal research doublet established at a site within the Northeast German Basin.

During a maximum of 6 months of flow no significant change in permeability in either direction was observed. Additionally, no negative effect of baryte precipitation or the exchange of the formation fluid against oxygen-rich water was encountered.

Despite significant differences in experimental strategy, some of the observations made are in agreement with the results obtained by [Tenthorey et al. \(1998\)](#). At moderate temperatures, samples rich in quartz will show no permeability damage, unless the composition of an externally introduced fluid allows authigenic mineral precipitation. Even with high feldspar contents their experiments demonstrated that the observed permeability decrease stopped only after a few days as a result of their closed fluid-rock system reaching equilibrium.

In the present study, the fluid has been continuously replaced as is the case within the reservoir during production. Further investigations should therefore address more systematically the effect of rock feldspar content, fluid composition, and flow-rate for both open and closed fluid systems in comparison.

Finally, a comparative study should be undertaken on both diagenetically consolidated rock samples and specimens made from compacted mineral sands having a similar composition. Here, differences in reactive surface area and surface energy could significantly affect the style and the degree of secondary mineral precipitation potentially leading to permeability damage.

Acknowledgments The authors thank Jörn Bartels, GTN-Neubrandenburg, for constructive discussions in the course of this study and Heinz Holl, GFZ Potsdam, for the petrographic interpretation of the rock microstructure. The chemical analysis of the fluid samples was performed by Petra Steinbach, VKTA Rossendorf e.V. Stefan Gehrman is thanked for the preparation of the thin-sections, and Helga Kemnitz and Juliane Herwig for their assistance with the SEM. The suggestions made by two anonymous reviewers helped to improve the manuscript. This research project was financially supported by the Federal Ministry for the Environment, Nature Conservation and Nuclear Safety under Grant No. BMU 0329951B.

References

- Aharonov, E., Tenthorey, E., Scholz, C.H.: Precipitation sealing and diagenesis: 2. Theoretical analysis. *J. Geophys. Res.* **103**(B10), 23969–23981 (1998). doi:[10.1029/98JB02230](#)
- Bear, J.: Dynamics of fluids in porous media. Dover Publication, Inc., Mineola, NY (1988)
- Blöcher, G., Moeck, I., Milsch, H., Zimmermann, G.: Modelling of pore pressure response due to hydraulic stimulation treatments at the geothermal research doublet EGrSk3/90 and GtGrSk4/05 in summer 2007. In: Proceedings, 33rd Workshop on Geothermal Reservoir Engineering, Stanford University, Stanford, California, SGP-TR-185 (2008)
- Darcy, H.: Les fontaines publique de la ville de Dijon. Dalmont, Paris (1856)
- De Boer, R.B., Nagtegaal, P.J.C., Duyvis, E.M.: Pressure solution experiments on quartz sand. *Geochim. Cosmochim. Acta* **41**, 257–264 (1977). doi:[10.1016/0016-7037\(77\)90233-2](#)
- Dunn, K., Daniel, E., Shuler, P.J., Chen, H.J., Tang, Y., Yen, T.F.: Mechanisms of surface precipitation and dissolution of baryte: a morphology approach. *J. Colloid Interface Sci.* **214**(2), 427–437 (1999). doi:[10.1006/jcis.1999.6224](#)
- Giese, L., Seibt, A., Wiersberg, T., Zimmer, M., Erzinger, J., Niedermann, S., et al: Geochemie der Formationsfluide. In: Huenges, E., Hurter, S. (eds.) In-situ Geothermielabor Groß Schönebeck: Bohrarbeiten, Bohrlochmessungen, Hydraulik, Formationsfluide, Tonminerale. Scientific Technical Report, STR02/14, GeoForschungsZentrum Potsdam, Potsdam, Germany (2002)
- Giger, S.B., Tenthorey, E., Cox, S.F., Fitz Gerald, J.D.: Permeability evolution in quartz fault gouges under hydrothermal conditions. *J. Geophys. Res.* **112**, B07202 (2007). doi:[10.1029/2006JB004828](#)

- Gratier, J.P., Guiguet, R.: Experimental pressure solution-deposition on quartz grains: the crucial effect of the nature of the fluid. *J. Struct. Geol.* **8**(8), 845–856 (1986). doi:[10.1016/0191-8141\(86\)90030-1](https://doi.org/10.1016/0191-8141(86)90030-1)
- Kühn, M., Frosch, G., Kölling, M., Kellner, T., Althaus, E., Schulz, H.D.: Experimentelle Untersuchungen zur Barytübersättigung einer Thermalsole. *Grundwasser* **3**, 111–117 (1997)
- Legarth, B., Huenges, E., Zimmermann, G.: Hydraulic fracturing in a sedimentary geothermal reservoir: results and implications. *Int. J. Rock Mech. Min. Sci.* **42**, 1028–1041 (2005). doi:[10.1016/j.ijrmmms.2005.05.014](https://doi.org/10.1016/j.ijrmmms.2005.05.014)
- Lemée, C., Guéguen, Y.: Modelling of porosity loss during compaction and cementation of sandstones. *Geology* **24**, 875–878 (1996). doi:[10.1130/0091-7613\(1996\)024<0875:MOPLDC>2.3.CO;2](https://doi.org/10.1130/0091-7613(1996)024<0875:MOPLDC>2.3.CO;2)
- Marty, N.S., Garboczi, E.J.: Length scales relating the fluid permeability and electrical conductivity in random two-dimensional porous media. *Phys. Rev. B* **46**, 6080–6090 (1992). doi:[10.1103/PhysRevB.46.6080](https://doi.org/10.1103/PhysRevB.46.6080)
- Milsch, H., Spangenberg, E., Kulenkampff, J., Meyhöfer, S.: A new apparatus for long-term petrophysical investigations on geothermal reservoir rocks at simulated in-situ conditions. *Transp. Porous Med.* **74**, 73–85 (2008). doi:[10.1007/s11242-007-9186-4](https://doi.org/10.1007/s11242-007-9186-4)
- Moeck, I., Schandelmeier, H., Holl, H.-G.: The stress regime in a Rotliegend reservoir of the Northeast German Basin. *Int. J. Earth Sci.* (2008). doi:[10.1007/s00531-008-0316-1](https://doi.org/10.1007/s00531-008-0316-1)
- Omar, A.E.: Effect of brine composition and clay content on the permeability damage of sandstone cores. *J. Petrol. Sci. Eng.* **4**, 245–256 (1990). doi:[10.1016/0920-4105\(90\)90014-T](https://doi.org/10.1016/0920-4105(90)90014-T)
- Rutter, E.H.: The kinetics of rock deformation by pressure solution. *Philos. Trans. R. Soc. London. Ser. A* **283**, 203–219 (1976)
- Scheidegger, A.E.: The physics of flow through porous media. University of Toronto Press, Toronto (1974)
- Seibt, A.: Welche Faktoren können die Eisen(II)-Oxidation in Formationswässern beeinflussen? In: Huenges, E. (ed.) *Geothermische Energieentwicklung—geologische und energietechnische Ansatzpunkte*. Scientific Technical Report, STR00/23, GeoForschungsZentrum Potsdam, Potsdam, Germany (2000)
- Small, J.S., Hamilton, D.L., Habesch, S.: Experimental simulation of clay precipitation within reservoir sandstones: 1. Techniques and examples. *J. Sediment. Petrol.* **62**, 508–519 (1992)
- Sprunt, E.S., Nur, A.: Destruction of porosity through pressure solution. *Geophysics* **42**, 726–741 (1977). doi:[10.1190/1.1440742](https://doi.org/10.1190/1.1440742)
- Tada, R., Maliva, R., Siever, R.: A new mechanism for pressure solution in porous quartzose sandstone. *Geochim. Cosmochim. Acta* **51**, 2295–2301 (1987). doi:[10.1016/0016-7037\(87\)90282-1](https://doi.org/10.1016/0016-7037(87)90282-1)
- Tenthorey, E., Scholz, C.H., Aharonov, E., Léger, A.: Precipitation sealing and diagenesis: 1. Experimental results. *J. Geophys. Res.* **103**(B10), 23951–23967 (1998). doi:[10.1029/98JB02229](https://doi.org/10.1029/98JB02229)
- Terzaghi, K.: Die Berechnung der Durchlässigkeitsziffer des Tones aus dem Verlauf der hydrodynamischen Spannungserscheinungen. *Sitz. Akad. Wiss. Wien, Math. Naturwiss. Kl., Abt. IIa* **132**, 105–124 (1923)
- Yasuhara, H., Polak, A., Mitani, Y., Grader, A.S., Hallek, P.M., Elsworth, D.: Evolution of fracture permeability through fluid-rock reaction under hydrothermal conditions. *Earth Planet. Sci. Lett.* **244**, 186–200 (2006). doi:[10.1016/j.epsl.2006.01.046](https://doi.org/10.1016/j.epsl.2006.01.046)